IEEE Access
Multidisciplinary | Rapid Review | Open Access Journal

Received July 8, 2019, accepted July 18, 2019, date of publication July 22, 2019, date of current version August 7, 2019.

*Digital Object Identifier 10.1109/ACCESS.2019.2930327*

# Folded Chirp-Rate Shift Keying Modulation for LEO Satellite IoT

**CHAO YANG[1], MEI WANG[2], LIN ZHENG[1,3], AND GUANGPENG ZHOU[1]**

[1]Guangxi Key Laboratory of Wireless Wideband Communications and Signal Processing, Guilin University of Electronic Technology, Guilin 541004, China
[2]Institution of Information Science and Engineering, Guilin University of Technology, Guilin 541004, China
[3]Science and Technology on Communication Networks Laboratory, Shijiazhuang 050081, China

Corresponding author: Mei Wang (mwang@glut.edu.cn)

This work was supported in part by the National Natural Science Foundation of China under Grant 61771151 and Grant 61761014, in part by the Guangxi Key Laboratory of Wireless Wideband Communication and Signal Processing under Grant GXKL061501, and in part by the Science and Technology on Communication Networks Laboratory under Grant KX172600033.

**ABSTRACT** In the low earth orbit (LEO) satellite Internet of Things (IoT), the IoT devices can be distributed in remote areas (e.g., desert, ocean, and forest) for some special applications, where they are unable to have direct terrestrial network accesses and can only be covered by satellite. But in the LEO satellite scenario, it has to face the effects of high doppler and fast doppler rate, due to satellite movement at high speed and utilization of higher frequency bands. So fine frequency synchronization and frequency track are necessary to be done, even for LORA. In this paper, we propose a folded chirp-rate shift keying (FCrSK) modulation with strong immunity to doppler effect. Its data information is mapped to different folded chirp-rate waveforms, which have an advantage of the consistency of bandwidth and symbol length among chirp-rates compared to traditional chirp-rate shift keying system. Moreover, we analyze the optimal non-coherent receiver in case of the doppler channel, whose optimal decision depends on signal energy focusability in frequency spectrum after dechirp, so frequency peak average rate adopts as a decision criterion. Furthermore, system parameters' setting is discussed so as to maximize system modulation efficiency with the minimum interference among chirp-rate. Finally, some simulations are provided to analyze robustness to doppler shift and doppler-rate in the system. And based on universal software radio platform (USRP), some experimental measurements are made to validate its feasibility under the realistic wireless environment and doppler environment.

**INDEX TERMS** Chirp rate shift keying (CrSK), chirp spread spectrum (CSS), Internet of Things (IoT), LORA, low-Earth orbit (LEO) satellites.

## I. INTRODUCTION

With the technology development of low-power wide-area network, the Internet of things application has emerged in every corner of human activity. However, due to the deployment limitation of terrestrial base transceiver stations (BTS), a terrestrial network is impossible or impractical to extend the coverage in remote areas (e.g. desert, ocean, forest, etc).

A possible solution to the specific problem of deployment is the provision of a low-Earth orbit (LEO) constellation of satellites [1], [2]. Compared to terrestrial networks, it has a larger covered scope so that can achieve global coverage, and provides a larger system capacity due to wider available frequency spectrum in satellite system. Besides, it owns also higher survivability against all kinds of natural disasters, such as Earthquakes, floods, typhoons, etc. On the other hand, LEO satellites has advantages of lower transmission delay and smaller transmission loss than Geosynchronous Earth Orbit (GEO) satellites.

But since the relative motion between the satellite and the user terminal, it has to solve the problem of high doppler shift [3], [4] and doppler rate [5], especially in Ku or Ka-band SatCom scenarios. As two core technologies in the Internet of things, NB-IoT and LORA have started some researches on sensitivity to doppler [6], [7]. In NB-IoT system, it is necessary to use auxiliary data for doppler estimation and compensation [8], [9]. In LORA system, it has some robustness to doppler shift [10]. But in LEO satellites, fine frequency synchronization is still necessary to eliminate high doppler shift for LORA, and the LoRa modulation was not designed

The associate editor coordinating the review of this manuscript and approving it for publication was Qiang Yang.

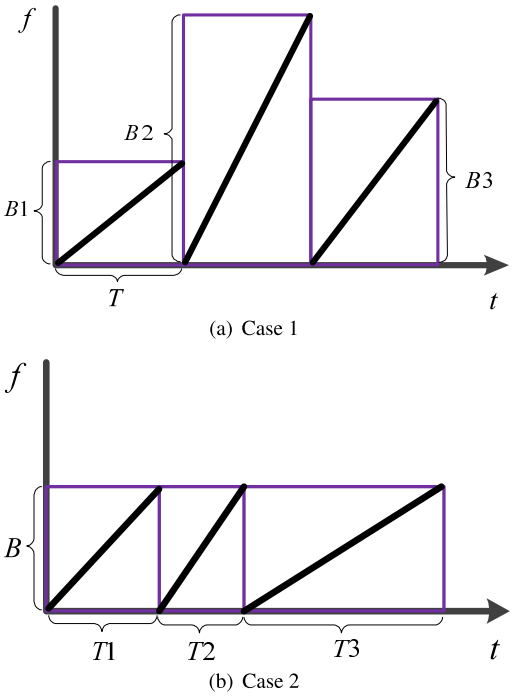


**FIGURE 1.** Time-frequency structure of traditional CrSK.

itself to deal with doppler rate. Hence, some researches on LORA have recently been carried out for LEO satellites. To cope with the high doppler shift and doppler rate, a new receiver architecture based on LORA is proposed for LEO satellite [11]. And based on analysis of correlation function, a symmetry chirp spread spectrum waveform is designed for LEO satellite [12], but the modulation is still regarded as a combination of frequency shift keying and chirp spread spectrum, so its robustness to doppler shift is similar with LORA's. Actually, LORA system mainly utilizes its spreading gain to improve SNR at receiver, but do not take full advantage of the time-frequency structure characteristics of chirp-rate, which has a potential advantage against doppler effect.

Early, some researchers propose a chirp-rate shift keying modulation based on Fractional Fourier Transform (FRFT), and point out that it owns an inherent immunity against doppler shift [13]. But different chirp-rate signals exist interference with each other in the FRFT domain [14], [15]. Although a chirp-rate modulation based on Bi-orthogonal Fourier Transform (BFT) is proposed subsequently, which can keep orthogonality of chirp-rate modulated with each other. Unfortunately, doppler interference dramatically limits its performance [16], [17]. Besides, above systems still exist a common problem: They haven't a constant bandwidth and symbol rate yet that make it hard to be implemented in practical communication system. The time-frequency structure of traditional CrSK is given as below:

*Case 1:* when chirp signals have identical symbol rate, its bandwidth occupied is not consistent for different chirp-rate, meaning that spreading gains are not the same for different chirp-rate signals. And to avoid sampling distortion, system sampling rate must be high enough to satisfy the demand for the largest chirp-rate signal, virtually increasing the pressure on ADC.

*Case 2:* when chirp signals have identical bandwidth, their symbol length aren't consistent for different chirp-rate, which results in uncertain symbol rate and increases the difficulty of symbol synchronization in receiver.

All in all, traditional CrSK system without constant bandwidth and symbol rate is very detrimental to system designing and signal processing. In this paper, a folded chirp waveform (FCW) is designed to modulate different chirp-rate signals on the constrain of constant bandwidth and symbol length. Moreover, a chirp-rate shift keying system is proposed based on FCW, called as FCrSK in this paper. Then we analyze the optimal non-coherent receiver in doppler channel, and a decision criterion based on frequency peak average rate is given for FCrSK. Besides, we will optimize system parameters so as to minimize interference among chirp-rates while realize maximum modulation efficiency. Furthermore, some simulations are provided to analyze robustness to doppler shift and doppler-rate in the system. And based on USRP, some experimental measurements are made to validate its feasibility in the realistic wireless environment and doppler environment.

The rest of the paper is organized as follows. In section II, we firstly illustrate construction of FCW. In section III, we provide a CRSK system based FCW, and present detailed derivation about modulation and demodulation, including analysis of chirp-rate matching and chirp-rate mismatching condition, selection of system parameters as well as analysis of the modulation efficiency. In section IV, some numerical simulation is provided to analyze robustness against doppler shift and an experimental measurement is made to test its performance under the actual wireless environment. Finally in Section V, we draw the conclusions of the paper.

## II. FOLDED CHIRP WAVEFORM

### A. WAVEFORM GENERATION

The continuous waveform of FCW is given by

$$s_{FCW}(t)=\sum_{d=0}^{D-1} rect(t-dT_c)e^{j(\pi \frac{B}{T_c}t^2-2\pi dBt)}, \quad 0 \le t < T, \tag{1}$$

where

$$rect(t) = \begin{cases} 1 & 0 \le t < T_c, \\ 0 & else. \end{cases}$$

It is a combination of $D$ chirp-chips within symbol length $T$ and bandwidth $B$, where a complete of chirp-chip is $T_c$ in length, and its index of chirp-chip is $d = 0, 1, \ldots, D-1$, as shown in Fig.2. Note that if $T_c = T$, FCW would be degenerated to a chirp signal of chirp-rate $u_0 = B/T$. This chirp-rate is defined as the standard chirp-rate for convenience in this paper. At sampling frequency of $f_s = aB = 1/T_s$, its

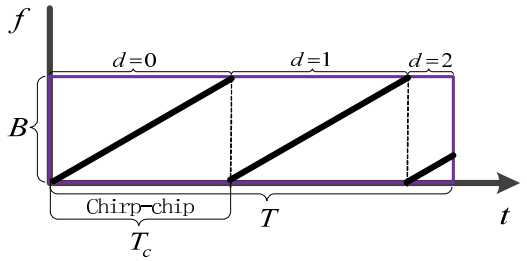


**FIGURE 2.** Time-frequency structure of FCW.

digital baseband signal can be expressed as

$$s_{FCW}(n) = \sum_{d=0}^{D-1} rect(nT_s - dMT_s)e^{j(\pi \frac{n^2}{aM} - 2\pi \frac{dn}{a})}, \quad 0 \le n \le N-1, \quad (2)$$

where $a$ is over-sampling factor and $T_s$ is sampling interval. $N$ and $M$ is sampling points of a symbol and a chirp-chip, respectively, and $M \in G = \{x | x \in [-N, N] \quad and \quad x \neq 0\}$.

Furthermore, Eq. 2 can be simplified at Nyquist sampling rate $f_s = N/T = B$

$$\begin{aligned} s_{FCW}(n) &= \sum_{d=0}^{D-1} rect(nT_s - dMT_s)e^{j\pi \frac{n^2}{M}} \\ &= e^{j\pi \frac{n^2}{M}} \quad 0 \le n \le N-1. \end{aligned} \quad (3)$$

Above simplified expression shows that digital FCW at Nyquist sampling rate $f_s = B$ has the same discrete expression as a digital chirp of bandwidth $B'$ (where $B' = BT/T_c > B$) at sub-Nyquist sampling rate $fs = B = B'M/N$. As shown in Fig.3, the discrete chirp in the blue ellipse has the same time frequency structure as the discrete FCW in the purple block at Nyquist sampling rate.

## III. FOLDED CHIRP-RATE SHIFT KEYING SYSTEM

### A. MODULATION AND DEMODULATION

In this section, we will introduce a folded chirp-rate shift keying (FCrSK) system based on FCW. In transmitter, data $x$ is mapped into a FCW through multiple chirp-rate selection module, as shown the flow on the left in Fig.4.

$$s_m(t) = \sum_{d=0}^{D-1} rect(t - dT_c)e^{j(\pi u_m t^2 - 2\pi dBt)} \quad 0 \le t < T, \quad (4)$$

where $u_m = mu_0$ is the chirp-rate of data $x$ mapping, and $m$ is a multiple of standard chirp-rate $u_0$.

After ideal time synchronization at the receiver, its digital baseband signal sampled by $f_s = B$ can be expressed as

$$r(n) = e^{j\pi \frac{m}{N} n^2} \quad 0 \le n \le N-1, \quad (5)$$

In order to recognize the chirp-rate, receiving signal need use all the possible FCW modulated as reference signals to dechirp processing on multi-channels, where reference signal of chirp-rate $u'_m = m'u_0$ is given by

$$s_{ref}(n) = e^{j\pi \frac{m'}{N} n^2} \quad 0 \le n \le N-1, \quad (6)$$

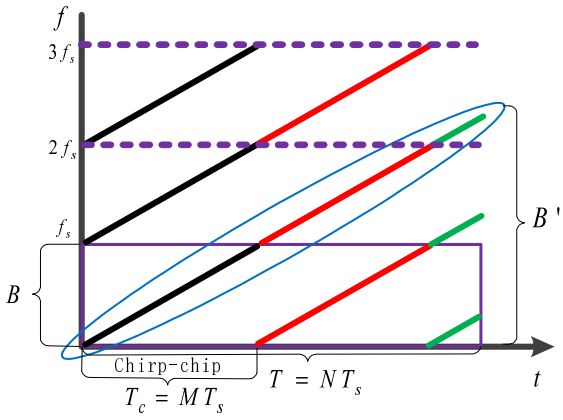


**FIGURE 3.** Time-frequency structure of discrete FCW at Nyquist sampling rate.

where the relationship between the samples $M'$ in a chirp-chip and the multiple $m'$ of standard chirp-rate is $M' = N/m'$.

Then operation of dechirp is taken

$$\begin{aligned} s_{dechirp}(n) &= r(n)s_{ref}(n)^* \quad 0 \le n \le N-1, \\ &= e^{j\pi \frac{m-m'}{N} n^2} \end{aligned} \quad (7)$$

where "*" is conjugate operation.

Considering that difference between $m$ and $m'$ influences the results of dechirp, the following discussion is divided into two cases.

*Case 1:* $m - m' = 0$, namely chirp-rate matching condition. In this case, only the DC component is left after dechirp. So its energy can be accumulated at zero frequency point by FFT and its magnitude in frequency domain satisfies

$$|s_{FFT\_match}(l)| = \begin{cases} N & l = 0 \\ 0 & else. \end{cases} \quad (8)$$

*Case 2:* $m - m' \neq 0$, namely chirp-rate mismatching condition.

In this case, Eq.7 reflects the impact of interference between different chirp-rate modulation signals. The interference presents the feature of a chirp signal, so its signal energy scatters over frequency domain, and the energy distribution depends on the difference between $m$ and $m'$.

Let $\Delta m = m - m'$, its result after FFT is below

$$S_{FFT\_mismatch}(l) = \sum_{n=0}^{N-1} e^{j\pi \frac{\Delta m}{N} n^2} e^{-j2\pi \frac{l}{N} n}, \quad 0 < l \le N-1. \quad (9)$$

Above equation can be seen as discrete chirp fourier transform (DCFT) [18], which has a property as below

*Lemma 1:* When the time bandwidth product $N$ is a prime at Nyquist sampling $f_s = B$, we have the following identity:

$$|\sum_{n=0}^{N-1} e^{\pm j\frac{2\pi}{N}(pn^2+qn)}| = \sqrt{N}, \quad 0 < p \le N-1, \quad p, q \in Z, \quad (10)$$

where $Z$ represents the set of integers.

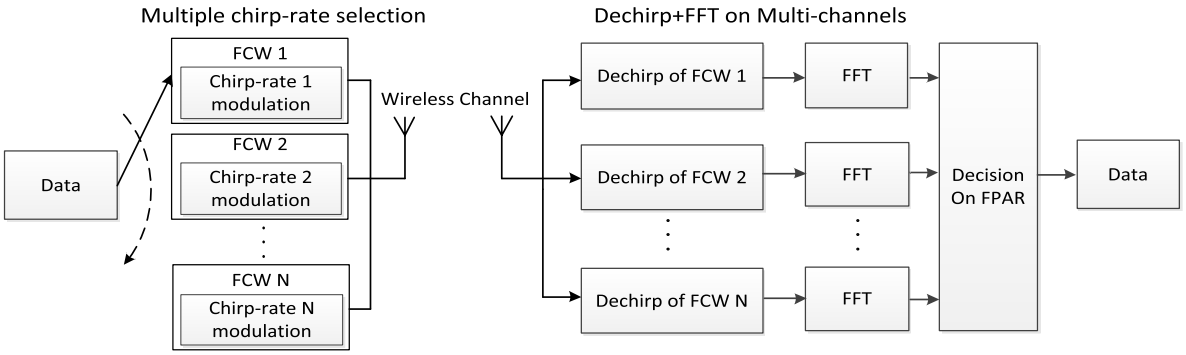


**FIGURE 4.** Signal processing flow chart of FCrSK system.

It indicates that signal energy under chirp-rate mismatching condition has a constant envelope $\sqrt{N}$ in frequency domain, when $N$ is a prime and $0 < |\Delta m| = 2p \leq 2N-2$ in $\Delta m \in Z$.

$$|S_{FFT\_mismatch}(l)| = \sqrt{N}, \quad 0 < l \leq N-1 \\ 0 < |\Delta m| \leq 2N-2 \quad \Delta m \in Z. \tag{11}$$

So when the time bandwidth product of FCW transmitted is a prime and its chirp-rate is odd or even times of standard chirp-rate, signal energy from chirp-rate mismatching can be uniformly distributed into the total bandwidth $B$ at Nyquist sampling $f_s = B$, and their energy is the same for all chirp-rate mismatching conditions. If above conditions are not met, signal energy from different chirp-rate mismatching is different, and maximum of its energy must be bigger than $\sqrt{N}$.

By comparison between case 1 and case 2, the decision on chirp-rate can be made by magnitude at zero frequency point after dechirp, which is actually an optimal non-coherent detection with unknown channel phase response $\theta$ in the case of AWGN [19], namely its decision rule is to maximize

$$\max_{0 \leq m \leq M-1} |\sum_{n=0}^{N-1} r(n) s_m^*(n)|.$$

However, it is not suitable to be used in doppler shift environment.

### B. EFFECT OF DOPPLER SHIFT

In AWGN channel, receiving signal with doppler shift can be expressed as

$$\mathbf{r} = g \Lambda_{\mathbf{w}} \mathbf{s_m} + \mathbf{n}, \tag{12}$$

where

$$g = Ae^{j\theta} \\ \mathbf{r} = [r(0), r(1), \ldots, r(N-1)] \\ \mathbf{s_m} = [s_m(0), s_m(1), \ldots, s_m(N-1)] \\ \Lambda_{\mathbf{w}} = diag(1, e^{jwT_s}, e^{jw2T_s} \ldots, e^{jw(N-1)T_s})$$

and $\mathbf{n}$ is a vector of AWGN. Besides, both of unknown random variable $\theta$ and $w$ follow the uniform distribution from 0 to $2\pi$ and from 0 to $B$, respectively.

Thus decision rule is to maximize the likelihood function

$$\begin{aligned} f(\mathbf{r}|m) &= (\frac{1}{2\pi N_0})^N \int_0^B \frac{1}{B} \int_0^{2\pi} \frac{1}{2\pi} \\ &\quad \times exp(-\frac{1}{2N_0} \|\mathbf{r} - Ae^{j\theta} \Lambda_{\mathbf{w}} \mathbf{s_m}\|) d\theta dw \\ &= (\frac{1}{2\pi N_0})^N exp(-\frac{\|\mathbf{r}\|^2 + A^2 \|\mathbf{s_m}\|^2}{2N_0}) \\ &\quad \times \int_0^B \frac{1}{B} \int_0^{2\pi} exp(\frac{A}{N_0} Re[e^{-j\theta} \Lambda_{\mathbf{w}}^{\mathbf{H}} \mathbf{s_m^H} \mathbf{r}]) d\theta dw. \end{aligned} \tag{13}$$

This is the same as choosing $m$ to maximize the last term under the condition that all of $\mathbf{s_m}$ have the same energy

$$\begin{aligned} c &= \frac{1}{B} \int_0^B \int_0^{2\pi} exp(\frac{A}{N_0} Re[e^{-j\theta} \Lambda_{\mathbf{w}}^{\mathbf{H}} \mathbf{s_m^H} \mathbf{r}]) d\theta dw \\ &= \frac{1}{B} \int_0^B \int_0^{2\pi} exp(\frac{A}{N_0} Re[e^{-j\theta} \sum_{n=0}^{N-1} r(n) s_m^*(n) e^{-jwnT_s}]) d\theta dw \\ &= \frac{1}{B} \int_0^B I_0(\frac{A}{N_0} |\sum_{n=0}^{N-1} r(n) s_m^*(n) e^{-jwnT_s}|) dw \\ &= \frac{1}{B} \int_0^B I_0(\frac{A}{N_0} |F_m(w)|) dw, \end{aligned} \tag{14}$$

where $I_0(\cdot)$ is the zeroth order modified Bessel function of the first kind, and frequency spectrum after dechirp by $m$th reference signal is recoded as

$$F_m(w) = \sum_{n=0}^{N-1} r(n) s_m^*(n) e^{-jwnT_s}.$$

It indicates that the likelihood function value $f(\mathbf{r}|m)$ depends on the structure of frequency spectrum after dechirp. To further analyze the relationship between $w$ and maximum of $c$, an approximate discrete form of $c$ is given by

$$\begin{aligned} c &= \frac{1}{B} \int_0^B I_0(\frac{A}{N_0} |F_m(w)|) dw \\ &\approx \lim_{N \to \infty} \frac{1}{N} \sum_{k=0}^{N-1} I_0(\frac{A}{N_0} |F_m(k\Delta w)|) \end{aligned} \tag{15}$$

where $\Delta w = B/N$.

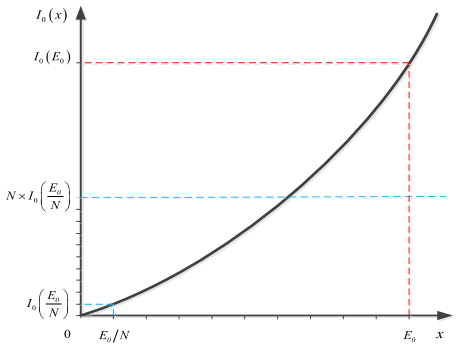


**FIGURE 5.** Zeroth order modified Bessel function of the first kind $I_0$.

Note that transmitted signal energy is limited, so sum of signal energy in the frequency domain is also limited after dechirp, namely $\sum_{k=0}^{N-1}|F_m(k\Delta w)| = E_0$. For convenience, the signal energy at $k$th frequency point after dechirp is denoted as $E_m(k) = |F_m(k\Delta w)|$, and constant factors are ignored. Thus, the maximization of Eq.15 is equivalent to

$$\widehat{m} = \max_{0\le m\le M-1}\sum_{k=0}^{N-1} I_0[E_m(k)] \tag{16}$$

where $E_m(k) \ge 0$ and $\sum_{k=0}^{N-1} E_m(k) = E_0$

Here, two extreme cases are discussed. One case is that all signal energy is concentrated at one frequency point, namely

$$E_m(k) = \begin{cases} E_0 & k \in [0, N-1] \\ 0 & else, \end{cases}$$

thus $\sum_{k=0}^{N-1} I_0[E_m(k)] = I_0(E_0)$. Moreover, the other case is that all signal energy is uniformly distributed in the whole frequency band, namely $E_m(k) = E_0/N$, thus $\sum_{k=0}^{N-1} I_0[E_m(k)] = NI_0(E_0/N)$. Furthermore, $I_0(x)$ is a monotonically increasing concave function, so $I_0(E_0) > NI_0(E_0/N_0)$, as shown in Fig.5.

It indicates that the likelihood function value $f(\mathbf{r}|m)$ corresponding to $F_m(w)$ of energy concentration is higher, and conversely, the one corresponding to $F_m(w)$ of energy dispersal is lower. This means that signal energy focusability in frequency spectrum after dechirp can be used as a decision for $\mathbf{s_m}$.

In FCrSK system, assuming that receiving signal exists doppler frequency of $f_d$, digital baseband signal sampled by $fs = B = 1/T_s$ in receiver can be expressed as

$$s_r(n) = e^{j\pi\frac{m}{N}n^2} e^{j2\pi f_d n T_s} \quad 0 \le n \le N-1, \tag{17}$$

where $f_d$ can be set to be $k$ times of fourier resolution $fs/N$, namely $f_d = kfs/N$.

So its result of dechirp is

$$s_{dechirp}(n) = e^{j\pi\frac{m-m'}{N}n^2} e^{j2\pi\frac{k}{N}n} \quad 0 \le n \le N-1. \tag{18}$$

In the case 1, its magnitude in frequency domain satisfies

$$|s_{FFT\_match}(l)| = \begin{cases} N & l = k \\ 0 & else. \end{cases} \tag{19}$$

Since that the peak position depends on doppler shift, a fixed frequency point is not suitable for decision. And from energy concentration of view, frequency peak average rate (FPAR) can be used as a decision criterion

$$FPAR_{match} = \frac{max(|s_{FFT\_match}(l)|)}{mean(|s_{FFT\_match}(l)|)} = N. \tag{20}$$

In the case 2, FCW signal energy in frequency domain after dechirp can be uniformly distributed into the total bandwidth $B$, and the characteristics of constant envelope in Eq.11 is not affected by doppler shift if $k \in Z$, so the lowest FPAR in frequency domain can be obtained

$$FPAR_{mismatch} = \frac{max(|s_{FFT\_mismatch}(l)|)}{mean(|s_{FFT\_mismatch}(l)|)} = 1. \tag{21}$$

It shows that chirp-rate decision based on FPAR is insensitive to doppler shift, so we can adopt FPAR as a decision in FCrSK system, as shown in Fig.4. But note that loss of sampling in frequency domain might occur due to the limitation of the resolution of Fourier transform. So if $k \notin Z$, it results in $FPAR_{mismatch} > 1$ and $FPAR_{FFT\_match} < N$.

### C. MODULATION EFFICIENCY

In order to reduce the interference between different chirp-rate signal, namely to get the lowest of FPAR in the case of chirp-rate mismatching, selection on chirp-rate in FCrSK system has some limitations as mentioned above: considering $|\Delta m| = 2p \le 2N-2$, $\Delta m \in Z$ and $N$ is a prime in Eq.11, that is, the time bandwidth product of FCW transmitted must be a prime and its chirp-rate must be integer times of standard chirp-rate $u_0$. Moreover, the difference between any two chirp-rate must be even times of standard chirp-rate $u_0$ and not exceed $2N-2$ times, so

$$u_{available} = (2c-1)u_0 \quad 0 \le |c| \le (N-1)/2,\ c \in Z,$$

or

$$u_{available} = 2cu_0 \quad 0 < |c| \le (N-1)/2,\ c \in Z.$$

Thus, maximum number of available chirp-rates is $N$ for FCrSK system, so each symbol can carry $log_2 N$ bits information. Moreover, bandwidth occupied for each FCW is $B = N/T$, and the Baud rate is $R = 1/T$, so the normalized bit rates of FCrSK is thus

$$\beta = \frac{R\log_2 N}{B} = \frac{\log_2 N}{N} \quad (Bit/s/Hz). \tag{22}$$

It shows that modulation efficiency of FCrSK is the same as LORA's [20].

## IV. PERFORMANCE ANALYSIS AND DISCUSSIONS

### A. NUMBERICAL SIMULATION

In this section, some simulations are provided to validate the feasibility of FCrSK system and analyze its robustness to doppler shift. The system parameters are given in Table 1:

Firstly, we show a transmitting FCW with $M = N/5$ in the Fig. 6, where a black line is the boundary between chirp-chips.

**TABLE 1. System parameters.**

| Parameters | Symbol | Value |
|---|---|---|
| Symbol Length | $T$ | 0.488ms |
| System Bandwidth | $B$ | 125kHz |
| Sampling Frequency | $f_s$ | 125kHz |
| Samples of a symbol | $N$ | 61 |
| Modulation Order | – | 61 |

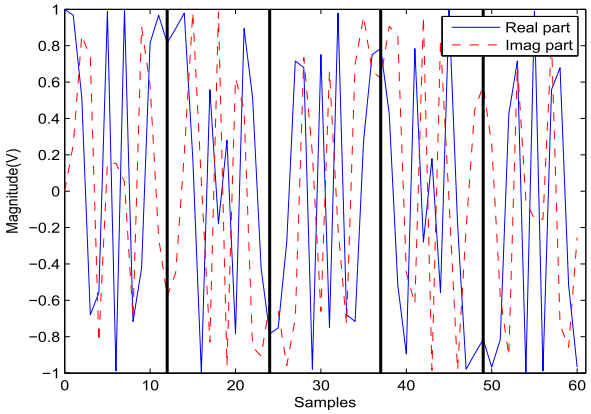


**FIGURE 6. Transmitting FCW with $M = N/5$.**

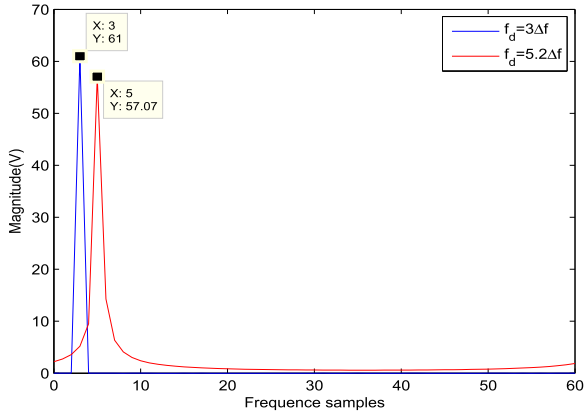


**FIGURE 7. Fourier spectrum of chirp-rate matching with $M = M' = N/5$.**

It can be seen that the FCW includes five chirp-chips, and phases between chirp-chips are continuous. Next, we will analyze the impact of doppler shift on FCW under condition of chirp-rate matching and mismatching. Here, doppler shift are assumed as $f_d$ and a frequency spacing unit $\Delta f$:

$$\Delta f = \frac{f_s}{N} = \frac{B}{N}$$

Fig. 7 shows a fourier spectrum from dechirp under the condition of chirp-rate matching. When doppler shift is the integer multiples of $\Delta f$, its magnitude at peak is N, which is consistent with Eq. 8. But when doppler shift is the non-integer multiples of $\Delta f$, it leads to loss of sampling due to the limitation of resolution of fourier transform, so its magnitude at peak is less than N.

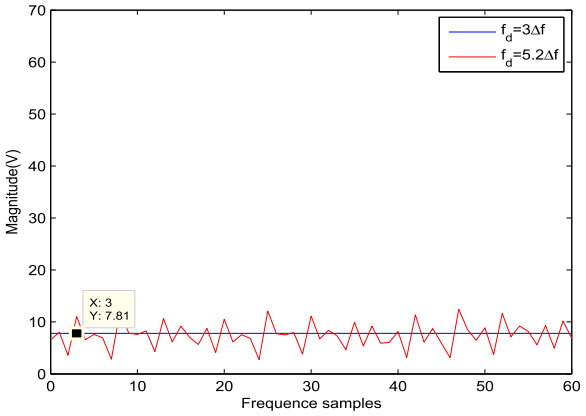


**FIGURE 8. Frequency spectrum of chirp-rate mismatching with $M = N/5$ and $M' = N/27$.**

On the other hand, Fig. 8 shows a frequency spectrum from dechirp under the condition of chirp-rate mismatching. When doppler shift is the integer multiples of $\Delta f$, it has a characteristic of constant envelope, and its magnitude is consistent with theoretical value $\sqrt{N} = 7.81$. But when doppler shift is the non-integer multiples of $\Delta f$, the spectrum turns up some fluctuation, as indicated in red line.

In general, interference energy in chirp-rate mismatch condition is dispersed over whole frequency domain so that maximum of the interference in frequency domain falls down. So both signal energy between chirp-rate matching and mismatching condition appear the evident difference in frequency domain, and they are not sensitive to doppler shift. Hence, FPAR can be used to effectively distinguish the chirp-rate matching and mismatching condition.

Afterwards, we give a performance comparison between FCrSK,FRFT-CrSK, MFSK and LORA without coding in Fig. 9. For the fair of the comparison, all systems adopt the same system parameters shown as Table I. Moreover, their modulation orders are all set to 61, where the number of available chirp-rates of FRFT-CrSK is also set to 61, and its chirp-rate is $u \in [-B/T : B/30T : B/T]$. Moreover, MFSK and LORA systems both are in 61 modulation orders. Besides, [15], [21] can be referenced to verify the rationality of simulation.

Since that different chirp-basis signals are orthogonal in LORA, but existing the interference in both CrSK. So we can see that BER performance in both CrSK are no better than LORA's under the AWGN and Doppler shift $f_d = 0$ environment. Moreover, the performance in FRFT-CrSK is worse than one in FCrSK. This is because chirp-rate interval of FRFT-CrSK are limited less than standard chirp-rate, resulting that its interference energy between different chirp-rates cannot be all flatten in the

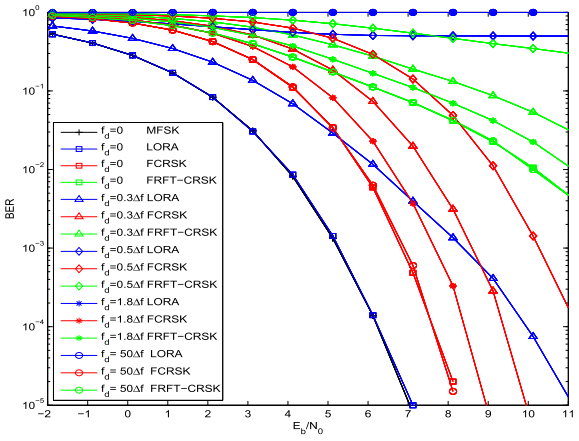


**FIGURE 9.** BER of LORA, FCrSK and FRFT-CrSK in different doppler frequency.

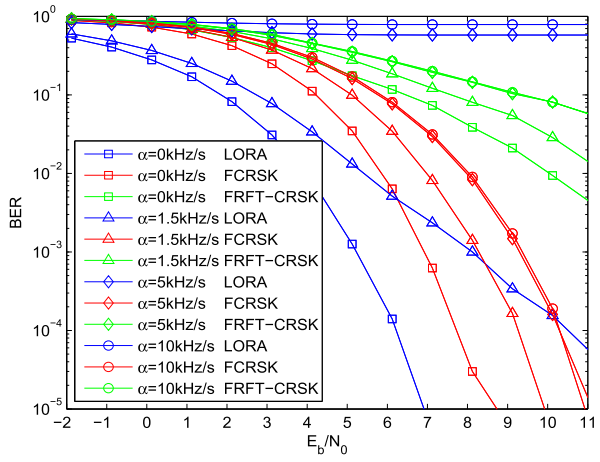


**FIGURE 10.** BER of LORA, FCrSK and FRFT-CrSK in different doppler-rate.

frequency domain. On the contrary, FCrSK can provide a bigger chirp-rate interval than standard chirp-rate so that its signal energy can be all dispersed over frequency domain to reach the minimum level of interference between chirp-rates, as shown in Fig.7.

On the other hand, it can be seen from doppler shift $f_d = 0.3\Delta f$ that LORA has certain ability to resist doppler shift, but it is not working correctly when $f_d \geq 0.5\Delta f$. That makes sense from that LORA can be seen as a structure of MFSK+Chirp [22], so it has a similar BER performance with MFSK. If once doppler shift is larger than half a frequency spacing $\Delta f$, its performance will rapidly deteriorate. But for both CrSK, their robustness to doppler is better than LORA's. Especially, FCrSK can still maintain a satisfactory performance at $E_b/N_0 = 11$. Besides, it is worth noting that FCrSK's performance at $f_d = 0.3\Delta f$ is worse than ones at $f_d = 1.8\Delta f$ and $f_d = 50\Delta f$, resulting from the frequency sampling loss, as shown in Fig.6 and Fig.7. Because the resolution of fourier transform is set to $\Delta f$, the closer doppler shift approaches an integral multiple of $\Delta f$, the system performance is better, so the system performance is worst when doppler shift is an half of $\Delta f$. Above results show that FCrSK's robustness to noise is superior to FRFT-CrSK's and it outperforms over LORA against large doppler shift. In other words, even without frequency synchronization, FCrSK can still provide a good performance under large doppler shift environment.

To further analyze the influences of doppler-rate on above systems, we provide a performance comparison in different doppler-rate for them, as shown in Fig.10. And to be fair, initial doppler shifts in three systems are set to zero for each frame, since that initial frequency synchronization can be done for each frame in LORA. Here we assume 1000 symbols as a frame, and doppler-rate $\alpha$ produces a doppler shift linearly increased with time in per frame [11].

So when $\alpha = 0\,Hz/s$, its performance is the same as one without doppler shift in Fig.9. But with the increase of doppler-rate, it leads to different degree of performance degradation for three systems. For example, when $\alpha = 1.5\,kHz/s$, maximum of doppler shift is no more than an half of frequency interval $\Delta f$ (namely $f_{dmax} = \alpha T = 732\,Hz \approx 0.357\Delta f$). In this case, FRFT-CRSK's performance is still worse than others, and FCrSK's performance is better than LORA's at high SNR ($E_b/N_0 > 8.5\,dB$). Instead, LORA is better at low SNR ($E_b/N_0 < 8.5\,dB$) due to the existence of interference among chirp-rates. Furthermore, when doppler-rate is further increasing, such as $\alpha = 5\,kHz/s$ and $\alpha = 10\,kHz/s$, maximums of doppler shift can reach $2.44\,kHz \approx 1.19\Delta f$ and $4.88\,kHz \approx 2.38\Delta f$. This means that the symbol sequence in LORA system can be shifted by one and two position at each frame, respectively. So it deteriorates seriously the performance in LORA. For both CrSK, the performance is better than LORA's. And since that the interference among chirp-rates in FCrSK is lower than FRFT-CrSK's, FCrSK shows a satisfactory performance at $E_b/N_0 = 11\,dB$, indicating that FCrSK has a good robustness to doppler shift and doppler-rate.

### B. EXPERIMENTAL MEASUREMENT

#### 1) MEASUREMENT IN THE WIRELESS ENVIRONMENT

To verify the feasibility of FCrSK system in the actual wireless environment, we built a 16-order FCrSK system based on universal software radio platform (NI USRP2953). Both omnidirectional antenna are equipped at transmitter and receiver, and realistic test scenario is shown in Fig.11.

Fig.12 and Fig.13 show both display interface of real-time signal processing at transmitter and receiver. And system parameters setting can be seen from the red box, including carrier frequency(2.4 $GHz$), symbol length(488 $us$) and system bandwidth(125 $kHz$). Besides, frequency stability of both devices is at 2.5 ppm.

Besides, signals are transmitted in frames, where each frame contains a data part of 16 symbols and a time

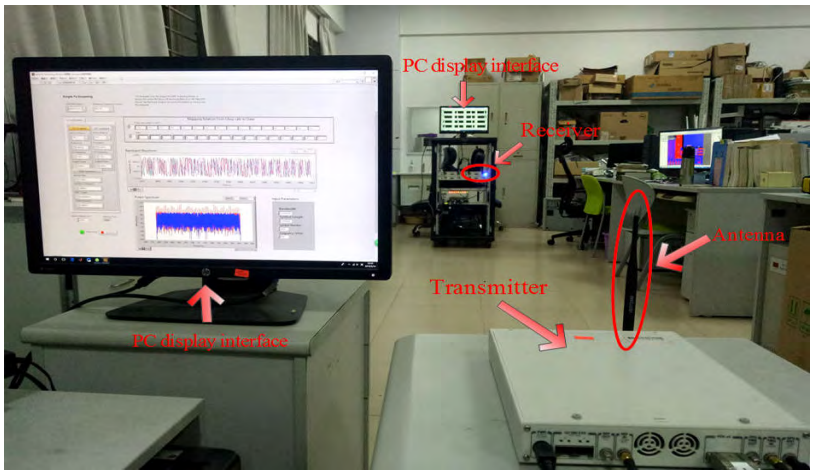


**FIGURE 11.** Realistic test scenario.

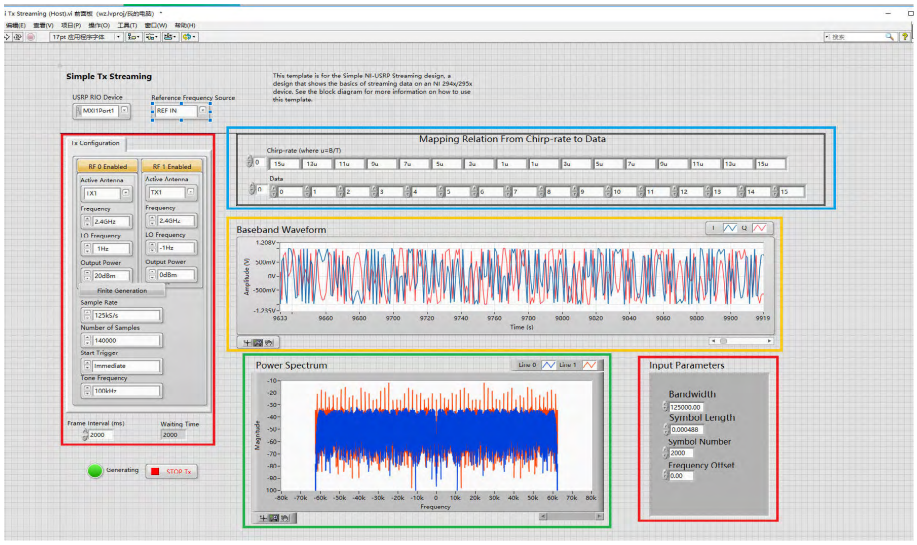


**FIGURE 12.** Display interface of real-time signal processing at transmitter.

synchronization part. For convenience of observation and analysis, data in each frame is set as $0-15$ in order. Moreover, the mapping relationships from chirp-rate to data are given in Fig.12 and Fig.13 by the blue box (where $u = B/T$ is standard chirp-rate). In Fig.12, the yellow box shows a baseband waveform of FCrSK transmitted. And green box shows its power spectrum, indicating that actual bandwidth occupied is 125 $kHz$.

In Fig.13(a), the yellow box and green box show baseband waveform of signal received and its power spectrum, respectively. In purple box, we show a frequency spectrum after dechirp in $9th$ chirp-rate channel, where the frequency spectrum is spliced in order from frequency spectrum of 16 symbols in every frame. Considering that frequency spectrum of a symbol contains 61 points and data is delivered in the order from 0 to 15, it is reasonable that matching peak occurs in the scope from 549 to 610. Beyond those, others are under mismatching condition, so their magnitudes are much low. On the other hand, frequency peak average rates of 16 symbols in every frame are shown in Fig.13(b), and it indicates that there is significant differentiation on FPAR under chirp-rate matching and chirp-rate mismatching condition. In the end, to reflect the stability of the system, we make a data statistic. And symbol error hasn't still occurred in a cumulative symbol number of 140000, as shown in Fig.13(a) by the black box.

### 2) MEASUREMENT ON THE ROBUSTNESS TO DOPPLER

To further verify robustness of FCrSK system to doppler shift, we built a test platform with RF channel emulator of Spirent VR5, as shown in Fig.14.

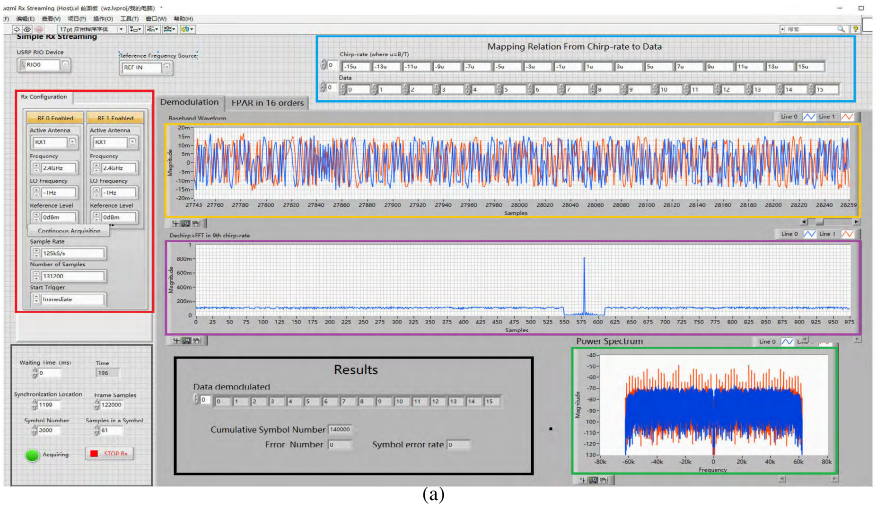


(a)

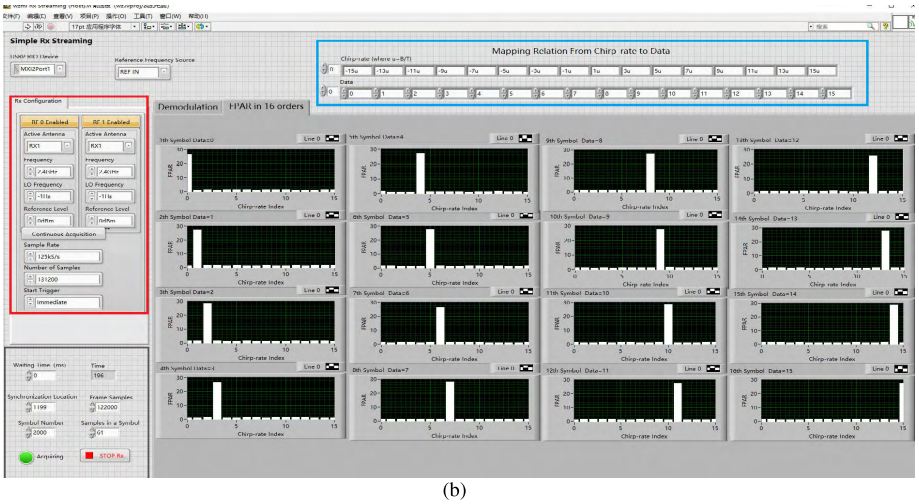


(b)

**FIGURE 13.** Display interface of real-time signal processing at receiver.

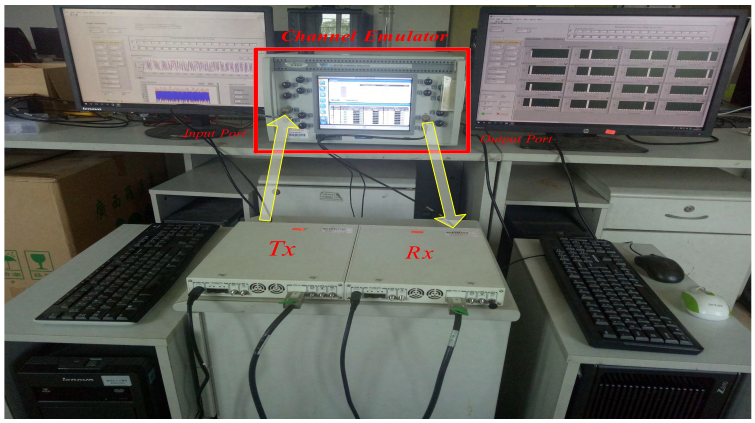


**FIGURE 14.** System test in doppler channel.

Seen from the figure, analog signal transmitted from TX is sent to RX through a channel emulator in red box.

In channel emulator, high speed train channel model is adopted [23]. And its parameters are shown in Fig.15, where maximum doppler shift is about 1.1 $kHz$. Besides, other system parameters are the same as ones in the wireless environment measurement, such as bandwidth, symbol length, carrier frequency, etc.

Finally, it can be seen from Fig. 16 that doppler shift has no remarkable influence on the symbol error rate and FPAR, indicating that system proposed has a good robustness to doppler shift.

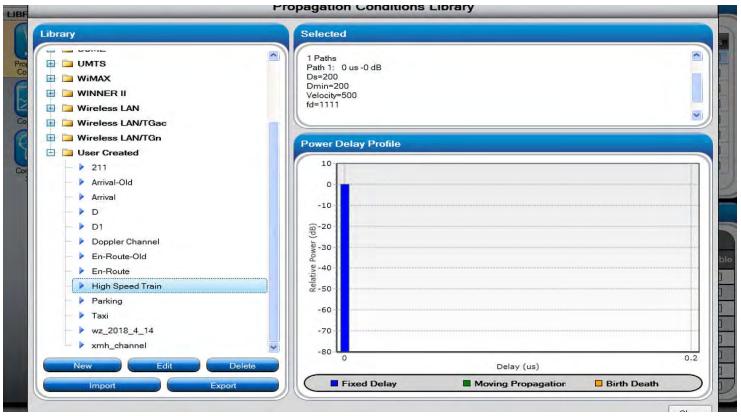


**FIGURE 15.** Channel parameters setting.

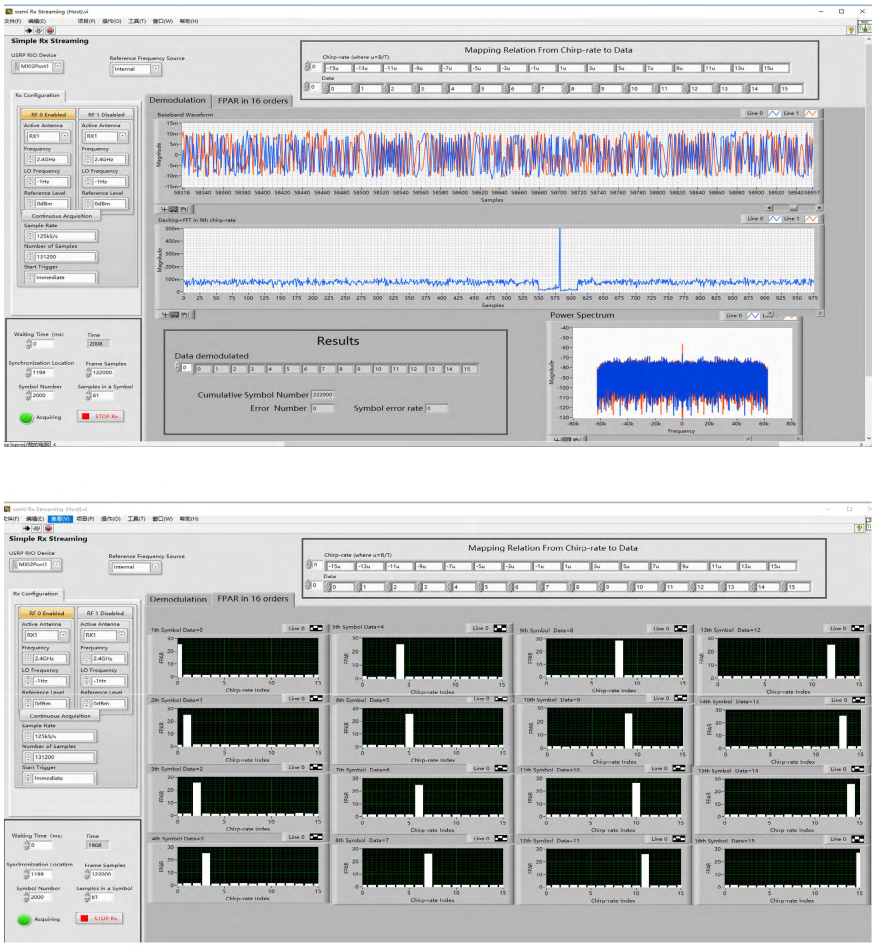


**FIGURE 16.** Display interface of real-time signal processing at receiver.

## V. CONCLUSION

In this paper, we propose a folded chirp shift keying system, whose modulation efficiency is the same as LORA's, but it has a stronger robustness to doppler shift than LORA's. Moreover, designing of folded chirp waveform solves a problem on inconsistency of bandwidth and symbol length among different chirp-rate from traditional CrSK. In demodulation, we derive analytically the optimal non-coherent receiver in doppler channel and draw a conclusion that its optimal decision depends on signal energy focusability in frequency spectrum after dechirp. So from energy concentration of view, a decision criterion is given based on FPAR. Besides, according to the property of DCFT, we point out some limiting conditions on selection of chirp-rate so as to

minimize interference among chirp-rates while realize maximum modulation efficiency.

In the end, simulation results show that FCrSK is a little worse than LORA without doppler shift due to the interference between different chirp-rates, but FCrSK outperforms over LORA against large doppler shift or large doppler-rate, and it has better robustness to noise than FRFT-CrSK. Furthermore, the feasibility of system is validated by experimental measurement in the realistic wireless environment and doppler environment.

Since the modulation scheme has strong immunity to doppler shift, thanks also to the intrinsic invariance of chirp-rate in the doppler effect, it maintains a satisfactory BER performance without frequency synchronization even when doppler is much large and variation of doppler is fast. So our proposed FCrSK system is suitable for LEO satellite-based IOT applications.

## REFERENCES

[1] Z. Qu, G. Zhang, H. Cao, and J. Xie, "Leo satellite constellation for Internet of Things," *IEEE Access*, vol. 5, pp. 18391–18401, 2017.

[2] O. Kodheli, A. Guidotti, and A. Vanelli-Coralli, "Integration of Satellites in 5G through LEO constellations," in *Proc. IEEE Global Commun. Conf.*, Dec. 2017, pp. 1–6.

[3] A. Guidotti, A. Vanelli-Coralli, M. Caus, J. Bas, G. Colavolpe, T. Foggi, S. Cioni, A. Modenini, and D. Tarchi, "Satellite-enabled LTE systems in LEO constellations," in *Proc. IEEE Int. Conf. Commun. Workshops*, May 2017, pp. 876–881.

[4] I. Ali, N. Al-Dhahir, and J. E. Hershey, "Doppler characterization for LEO satellites," *IEEE Trans. Commun.*, vol. 46, no. 3, pp. 309–313, Mar. 1998.

[5] M. Morelli, "Doppler-rate estimation for burst digital transmission," *IEEE Trans. Commun.*, vol. 50, no. 5, pp. 707–710, May 2002.

[6] Y. D. Beyene, R. Jantti, S. Iraji, and K. Ruttik, "On the performance of narrow-band Internet of Things (NB-IoT)," in *Proc. IEEE Wireless Commun. Netw. Conf. (WCNC)*, Mar. 2017, pp. 1–6.

[7] Y. Li, S. Han, L. Yang, F.-Y. Wang, and H. Zhang, "LoRa on the move: Performance evaluation of LoRa in V2X communications," in *Proc. 4th IEEE Intell. Vehicles Symp.*, Jun. 2018, pp. 1107–1111.

[8] Y. Zhou, J. Wang, and M. Sawahashi, "Downlink transmission of broadband OFCDM Systems-part II: Effect of Doppler shift," *IEEE Trans. Commun.*, vol. 54, no. 6, pp. 1097–1108, Jun. 2006.

[9] Z. Hou, Y. Zhou, L. Tian, J. Shi, Y. Li, and B. Vucetic, "Radio environment map-aided Doppler shift estimation in LTE railway," *IEEE Trans. Veh. Technol.*, vol. 66, no. 5, pp. 4462–4467, May 2017.

[10] J. Petäjäjärvi, K. Mikhaylov, M. Pettissalo, J. Janhunen, and J. Iinatti, "Performance of a low-power wide-area network based on LoRa technology: Doppler robustness, scalability, and coverage," *Int. J. Distrib. Sensor Netw.*, vol. 13, no. 3, pp. 1–16, 2017.

[11] G. Colavolpe, T. Foggi, M. Ricciulli, Y. Zanettini, and J.-P. Mediano-Alameda, "Reception of LoRa signals from LEO satellites," *IEEE Trans. Aerosp. Electron. Syst.*, to be published.

[12] Y. Qian, L. Ma, and X. Liang, "Symmetry chirp spread spectrum modulation used in LEO satellite Internet of Things," *IEEE Commun. Lett.*, vol. 22, no. 11, pp. 2230–2233, Nov. 2018.

[13] B. Deng, R. Tao, and E. Chen, "A novel method for binary chirp-rate modulation and demodulation," in *Proc. 8th Int. Conf. Signal Process.*, Nov. 2006, pp. 1–4.

[14] B. Deng, S. Cui, and X. Li, "Analysis of bandwidth efficiency and modulation parameter for chirp-rate modulation," in *Proc. 2nd Int. Conf. Meas., Inf. Control*, Aug. 2013, pp. 394–398.

[15] Q.-M. Zhao, Q.-Y. Zhang, and N.-T. Zhang, "Multiple chirp-rate modulation based on fractional Fourier transform," in *Proc. 1st Int. Conf. Pervasive Comput., Signal Process. Appl.*, Sep. 2010, pp. 688–691.

[16] L. Zheng, C. Yang, H. Qiu, and C. Yan, "Biorthogonal Fourier transform for multichirp-rate signal detection over dispersive wireless channel," *EURASIP J. Wireless Commun. Netw.*, vol. 1, pp. 1–13, Dec. 2018.

[17] H. Wang, Y.-H. Li, and B.-Q. Wang, "High-order Bi-orthogonal Fourier transform and its applications in non-stability signal analysis," *IEICE Trans. Inf. Syst.*, vol. 98, no. 1, pp. 189–192, Jan. 2015.

[18] X.-G. Xia, "Discrete chirp-Fourier transform," *Int. Soc. Opt. Photon.*, vol. 3810, pp. 27–38, Sep. 1999.

[19] T. F. Wong and T. M. Lok, *Theory of Digital Communication*. Gainesville, FL, USA: Univ. Florida, 2004, pp. 75–77, ch. 4.

[20] X. Ouyang, O. A. Dobre, Y. L. Guan, and J. Zhao, "Chirp spread spectrum toward the Nyquist signaling rate—Orthogonality condition and applications," *IEEE Signal Process. Lett.*, vol. 24, no. 10, pp. 1488–1492, Oct. 2017.

[21] Stack Exchange. (2018). *Conversion Between Eb/N0 and SNR in Spread-Spectrum Modulation Like LoRa CSS?*. Accessed: Jan. 8, 2018. [Online]. Available: https://dsp.stackexchange.com/questions/46239/conversion-between-eb-n0-and-snr-in-spread-spectrum-modulation-like-lora-css

[22] L. Vangelista, "Frequency shift chirp modulation: The LoRa modulation," *IEEE Signal Precess. Lett.*, vol. 24, no. 12, pp. 1818–1821, Dec. 2017.

[23] Group Radio Access Network, *Evolved Universal Terrestrial Radio Access(E-UTRA);Base Station(BS) Radio Transmission and Reception (Release 10)*, document SGPP TS36.104, 3GPP, 2010. [Online]. Available: https://www.docin.com/p-681527603.html

**CHAO YANG** was born in Shaanxi, China, in 1988. He received the M.S. degree in information and communication engineering from the Guilin University of Electronic Technology, Guilin, China, in 2015, where he is currently pursuing the Ph.D. degree. His research interests include broadband communications, MIMO communication, and radar-communication integration.

**MEI WANG** received the M.S. and Ph.D. degrees in electronic engineering from Xidian University, Xi'an, China, in 1989 and 2003, respectively. From 2003 and 2016, she was with the Guangxi Wireless Broadband Communication and Signal Processing Key Laboratory, Guilin University of Electronic Technology. In 2006, she was a Visiting Scholar with the University of Central Florida, Orlando. She is currently the Vice President with the Guilin University of Technology. Her research interests include sensor networks, location awareness, and cooperative location.

**LIN ZHENG** was with the CDMA Department of ZTE, in the development of CDMA2000 base station system, from 2000 to 2003. After that, he began a doctorate program in UWB at Xidian University, in 2003. He is currently a Professor with the Guangxi Key Laboratory of Wireless Wideband Communications and Signal Processing, Guilin University of Electronic Technology. His research interests are wireless sensor network, wireless network clock synchronization technology, and wireless ultra-wideband communications and location.

**GUANGPENG ZHOU** was born in Inner Mongolia, China, 1995. He received the B.S. degree in communication engineering from Liaoning Technical University, in 2018. He is currently pursuing the master's degree with the Guilin University of Electronic Technology, Guilin, China. His main research interest includes radar communication integration.